

The kaobook class

Use this document as a template

My PhD Thesis

Customise this page according to your needs

Tobias Hangleiter*

May 1, 2025

* A \LaTeX lover/hater

The kaobook class

Disclaimer

You can edit this page to suit your needs. For instance, here we have a no copyright statement, a colophon and some other information. This page is based on the corresponding page of Ken Arroyo Ohori's thesis, with minimal changes.

No copyright

© This book is released into the public domain using the CC0 code. To the extent possible under law, I waive all copyright and related or neighbouring rights to this work.

To view a copy of the CC0 code, visit:

<http://creativecommons.org/publicdomain/zero/1.0/>

Colophon

This document was typeset with the help of KOMA-Script and L^AT_EX using the kaobook class.

The source code of this book is available at:

<https://github.com/fmarotta/kaobook>

(You are welcome to contribute!)

Publisher

First printed in May 2019 by

The harmony of the world is made manifest in Form and Number, and the heart and soul and all the poetry of Natural Philosophy are embodied in the concept of mathematical beauty.

– D'Arcy Wentworth Thompson

Contents

Contents	v
I A FLEXIBLE PYTHON TOOL FOR FOURIER-TRANSFORM NOISE SPECTROSCOPY	1
1 Introduction	3
2 Theory of spectral noise estimation	5
2.1 Spectrum estimation from time series	6
2.2 Window functions	8
2.3 Welch's method	9
2.4 Parameters & Properties of the PSD	10
3 The python_spectrometer software package	13
3.1 Package design and implementation	13
3.1.1 Data acquisition	13
3.1.2 Data processing	15
3.2 Feature overview	16
3.2.1 Serial spectrum acquisition	17
3.2.2 Live spectrum acquisition	20
4 Conclusion and outlook	23
II CHARACTERIZATION AND IMPROVEMENTS OF A MILLIKELVIN CONFOCAL MICROSCOPE	27
5 Introduction	29
6 Characterization of electrical performance	31
6.1 Electron temperature	31
7 Characterization and improvements of the optical path	33
8 Vibration performance	35
8.1 Accelerometric vibration spectroscopy	35
8.2 Optical vibration spectroscopy	36
9 Conclusion & outlook	39
III OPTICAL MEASUREMENTS OF ELECTROSTATIC EXCITON TRAPS IN SEMICONDUCTOR MEMBRANES	41
IV A FILTER-FUNCTION FORMALISM FOR UNITAL QUANTUM OPERATIONS	43
10 Introduction	47
11 Filter function formalism for unital quantum operations	51
11.1 Transfer matrix representation of quantum operations	51
11.1.1 Brief review of quantum operations and superoperators	51
11.1.2 Liouville representation of the error channel	52

11.2	Calculating the decay amplitudes	57
11.2.1	Control matrix of a gate sequence	58
11.2.2	Control matrix of a single gate	60
11.3	Calculating the frequency shifts	61
11.4	Computing derived quantities	63
11.4.1	Average gate and entanglement fidelity	63
11.4.2	State fidelity and measurements	64
11.4.3	Leakage	64
11.5	Performance analysis and efficiency improvements	65
11.6	Periodic Hamiltonians	65
11.7	Extending Hilbert spaces	66
11.8	Operator bases	67
11.9	Computational complexity	68
12	Software implementation	73
12.1	Package overview	73
12.2	Workflow	74
13	Example applications	77
13.1	Singlet-triplet two-qubit gates	77
13.2	Rabi driving	79
13.3	Randomized Benchmarking	81
13.4	Quantum Fourier transform	84
14	Further considerations	87
15	Conclusion and outlook	89
16	Monte Carlo and Lindblad master equation simulations	91
16.1	Validation of QFT fidelities	91
17	Reconstruction by frequency-comb time-domain simulation	93
APPENDIX		95
A	Filter Functions	97
A.1	Additional derivations	97
A.1.1	Derivation of the single-qubit cumulant function in the Liouville representation	97
A.1.2	Evaluation of the integrals in Equation 11.39	98
A.1.3	Simplifying the calculation of the entanglement infidelity	98
A.2	Singlet-Triplet Gate Fidelity	99
A.3	GRAPE-optimized gate set for QFT	101
A.4	Convergence Bounds	102
A.4.1	Magnus Expansion	102
A.4.2	Infidelity	103
A.5	Second-order concatenation	104
List of Terms		105

List of Figures

2.1	Generated by <code>img/tikz/spectrometer/lockin_dut.tex</code>	5
2.2	Generated by <code>img/code/spectrometer/lorentz.py</code>	7
2.3	Generated by <code>img/code/spectrometer/pyspeck.py</code>	9
2.4	Generated by <code>img/code/spectrometer/pyspeck.py</code>	9
2.5	Generated by <code>img/code/spectrometer/pyspeck.py</code>	10
2.6	Generated by <code>img/tikz/spectrometer/daq_settings.tex</code>	11
3.1	Generated by <code>img/tikz/spectrometer/speck_tree.tex</code>	13
3.2	Generated by <code>img/code/spectrometer/pyspeck_workflow.py</code>	17
3.3	Generated by <code>img/code/spectrometer/pyspeck_workflow.py</code>	18
3.4	Generated by <code>img/code/spectrometer/pyspeck_workflow.py</code>	19
3.5	Generated by <code>img/code/spectrometer/pyspeck_workflow.py</code>	19
3.6	Generated by <code>img/code/spectrometer/pyspeck_workflow.py</code>	19
3.7	Generated by <code>img/code/spectrometer/pyspeck_workflow.py</code>	20
3.8	Generated by <code>img/code/spectrometer/pyspeck_live_view.py</code>	21
6.1	Generated by <code>img/code/setup/transport.py</code>	32
6.2	Generated by <code>img/code/setup/transport.py</code>	32
6.3	Generated by <code>img/code/setup/transport.py</code>	32
8.1	Generated by <code>img/code/setup/vibrations.py</code>	36
8.2	Generated by <code>img/code/setup/vibrations.py</code>	36
8.3	Generated by <code>img/code/setup/vibrations.py</code>	36
8.4	Generated by <code>img/code/setup/vibrations.py</code>	36
8.5	Generated by <code>img/code/setup/vibrations.py</code>	37
11.1	Illustration of gate sequence	59
11.2	Performance of the formalism using Equation 11.35 compared to a Monte Carlo method for a single gate as a function of problem dimension d . Parameters are: $n_{\Delta t} = 1, n_{\alpha} = 3, n_{MC} = 100, f_{UV} = 10^2/\Delta t, n_{\omega} = 500$ where n_{α} is the number of noise operators considered, n_{MC} the number of Monte Carlo trajectories over which is averaged, and n_{ω} the number of frequency samples. The calculation using filter functions clearly outperforms MC for small system sizes. For dimensions larger than $d \approx 100$ (roughly equivalent to 7 qubits) Monte Carlo (blue squares) performs better than the filter function (FF) calculation with transfer matrices (green triangles) for this set of parameters and processor due to the better scaling behavior. Using conjugation by unitaries (orange diamonds) significantly outperforms Monte Carlo (MC) also for large dimensions. While the fits to $t = ad^b$ (lines) underestimate the leading order exponent due to the data not being in the asymptotic regime, they support the expected relationship of complexity between the approaches. The inset shows the same data on a linear scale, highlighting the different scaling behaviors for large d	70
13.1	(a) Exchange interaction $J(\epsilon_{ij})$ for the CNOT gate presented in Reference Cerfontaine2020b as function of time. (b) Filter functions $F_{\epsilon_{ij}}$ for noise in the detunings evaluated on the computational subspace. The filter functions are modulated by oscillations at high frequencies due to numerical artifacts of the finite step size for the time evolution. The inset shows the filter functions in the DC regime on a linear scale with distinct peaks around $\omega = 2\pi/\tau$ and $\omega = 50/\tau$ ($\tau = 50$ ns). (c)–(e) Computational subspace block of the first order approximation of the error transfer matrix, given by the cumulant function $\mathcal{K}_{\alpha\alpha}$ excluding second order contributions, for the CNOT gate and the three detunings $\alpha \in \{\epsilon_{12}, \epsilon_{23}, \epsilon_{34}\}$. Note that in panel (e) the order of the rows and columns was permuted for better comparability.	79

13.2	Filter functions for weak (a) and strong (b) Rabi driving (20 identity gates in total). Grey dashed (dotted) lines indicate the respective drive (Rabi) frequencies ω_0 (Ω_R). (a) Weak driving with $A/\omega_0 \ll 1$. The filter function F_{xx} for noise operator σ_x is approximately constant up to the resonance frequency where it peaks sharply and then aligns with the filter function F_{zz} for σ_z . F_{zz} peaks at the Rabi frequency before rolling off with ω^{-2} and a DC level that is almost ten orders of magnitude larger than the DC level of the transverse filter function F_{xx} . (b) Strong driving with $A/\omega_0 \sim 1$. Again F_{zz} peaks at Ω_R whereas F_{xx} has three distinct peaks at ω_0 and $\omega_0 \pm \Omega_R$. These features also appear at slightly higher frequencies in F_{zz} due to the strong coupling.	81
13.3	Simulation of a standard randomized benchmarking (SRB) experiment using 100 random sequences per point for different gate and noise types (see the main text for an explanation of the gate type monikers). Dashed lines are fits of Equation 13.3 to the data while the solid black lines correspond to a zeroth-order SRB model with $A = B = 0.5$ and the true average gate infidelity per Clifford r . Errorbars show the standard deviation of the SRB sequence fidelities, illustrating that for the “single” gate set noise correlations can lead to amplified destructive and constructive interference of errors. The same noise spectrum is used for all three error channels ($\sigma_x, \sigma_y, \sigma_z$) and the large plots show the sum of all contributions. (a) Uncorrelated white noise with the noise power adjusted for each gate type so that the average error per gate r is constant over all gate types. No notable deviation is seen between different gate types. (b) Correlated $1/f$ -like noise with noise power adjusted to match the average Clifford fidelity in (a). The decay of the “single” gateset differs considerably from that of the other gate sets and the SRB decay expected for the given average gate fidelity, whereas “naive” and “optimized” gates match the zeroth order SRB model well, indicating that correlations in the noise affect the relation between SRB decay and average gate fidelity in a gateset-dependent way. Inset: contributions from σ_z -noise show that the sequence fidelity can be better than expected for certain gate types and noise channels.	84
13.4	quantum Fourier transform (QFT) circuit and filter function	86
A.1	Filter functions of the voltage detunings ϵ_{ij} excluding (a) and including (b) the zero-padded identity matrix basis element $C_0^c \propto \text{diag}(1, 1, 1, 1, 0, 0)$ for the computational subspace. Evidently, including C_0^c removes the DCG character, namely that $F_{\epsilon_{ij}}(\omega) \rightarrow 0$ as $\omega \rightarrow 0$, of the gates but has little effect on the high-frequency behavior. As the pulse optimization minimizes, among other figures of merit, the infidelity of the final propagator mapped to the closest unitary on the computational subspace due to quasistatic and fast white noise, this indicates that excluding C_0^c from the filter function corresponds to partially neglecting non-unitary components of the propagator on the computational subspace.	101
A.2	Control fields (top row) and corresponding filter functions (bottom row) of the GRAPE-optimized pulses in G. (a),(b) $X_0(\pi/2)$; (c),(d) $Y_0(\pi/2)$; (e),(f) $CR_{01}(\pi/2^3)$. Note that the optimization is neither very sophisticated nor realistic as the algorithm only maximizes the systematic (coherent) fidelity $\text{tr}(UQ_{\text{targ}}^\dagger)/d$ and the randomly distributed initial control amplitudes are not subject to any constraints.	102

Part I

**A FLEXIBLE PYTHON TOOL FOR
FOURIER-TRANSFORM NOISE
SPECTROSCOPY**

Part II

CHARACTERIZATION AND IMPROVEMENTS OF A MILLIKELVIN CONFOCAL MICROSCOPE

Introduction

5



Characterization of electrical performance

6



6.1 Electron temperature

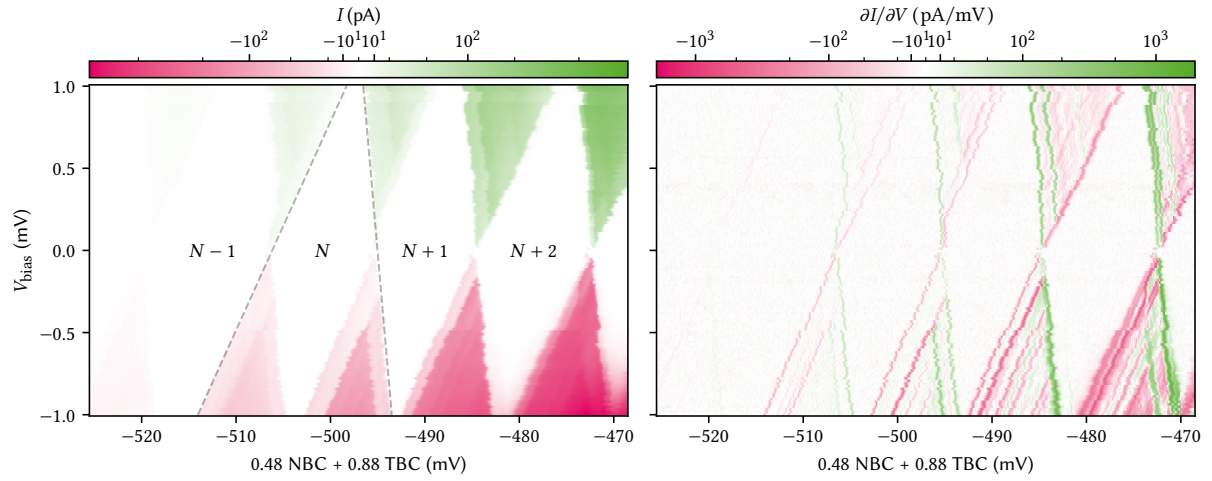


Figure 6.1

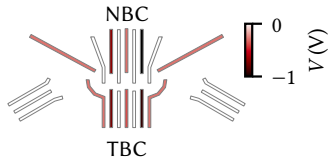


Figure 6.2

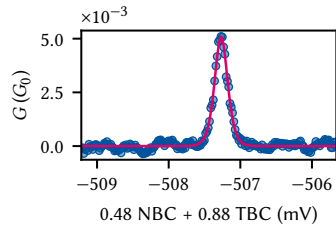


Figure 6.3

Characterization and improvements of the optical path

7



Vibration performance

8



8.1 Accelerometric vibration spectroscopy

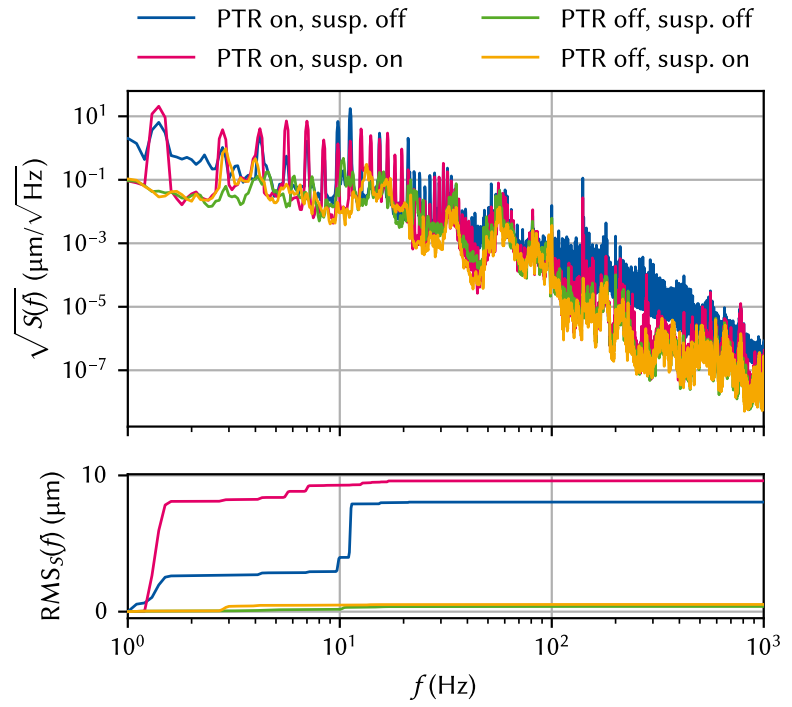


Figure 8.1

8.2 Optical vibration spectroscopy

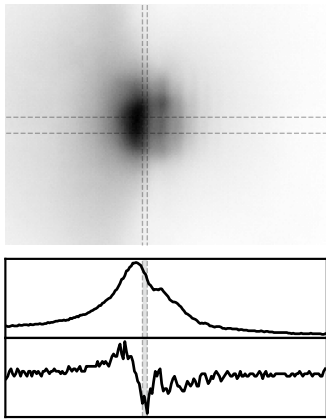


Figure 8.2

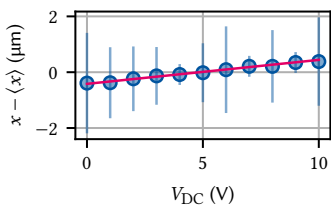
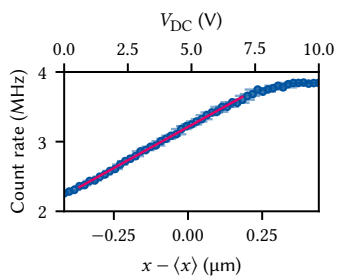


Figure 8.3



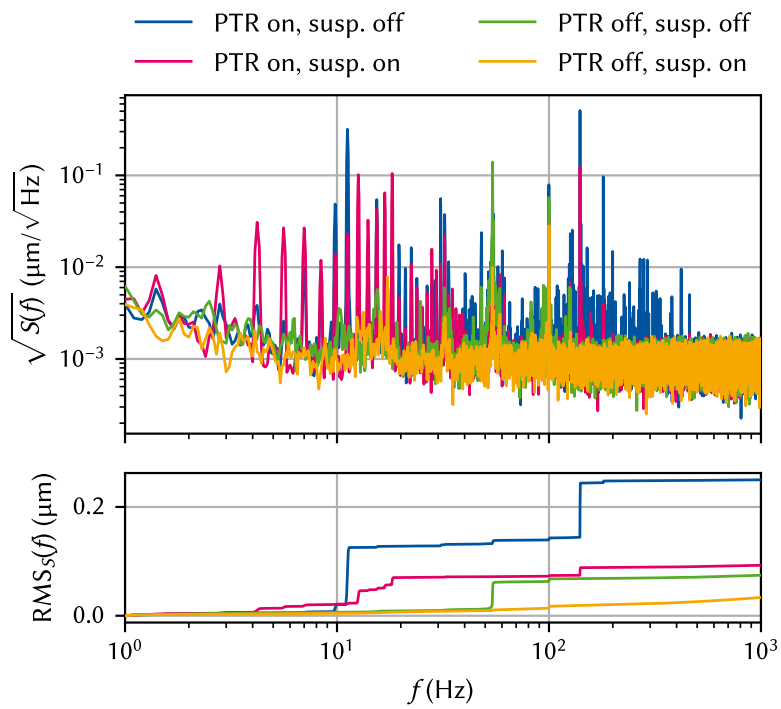


Figure 8.5

Conclusion & outlook

9



Part III

**OPTICAL MEASUREMENTS OF
ELECTROSTATIC EXCITON TRAPS IN
SEMICONDUCTOR MEMBRANES**

Part IV

A FILTER-FUNCTION FORMALISM FOR UNITAL QUANTUM OPERATIONS

APPENDIX

Special Terms

F

FF filter function. vii

M

MC Monte Carlo. vii

P

PSD power spectral density. v

Q

QFT quantum Fourier transform. viii

S

SRB standard randomized benchmarking. viii